

Abiotic drivers of a deep cyanobacteria layer in a stratified and eutrophic lake

Jacqueline Taylor¹, Miki Hondzo², and Vaughan R. Voller²

¹University of Minnesota, Twin Cities

²University of Minnesota

November 24, 2022

Abstract

Harmful algal blooms (HABs), in particular those consisting of the cyanobacteria *Microcystis*, are becoming increasingly more common across the globe. Despite the growing body of evidence that suggests vertical heterogeneity of *Microcystis* can be a precursor to HAB formation, the abiotic drivers of vertical distribution of *Microcystis* are poorly understood in the field environment. The prediction of subsurface cyanobacteria is also pertinent because subsurface concentrations are not easily recognizable to the public or lake system managers, creating an unnoticed safety hazard. High-frequency temporal and vertical data were collected from an Eulerian research station anchored in a stratified and eutrophic lake for five months. Data show that the magnitude of the subsurface *Microcystis* concentration peak and the center of gravity of the deep cyanobacteria layer are statistically significantly mediated by the thermal structure of the lake. The peak subsurface cyanobacteria biovolume scales linearly with the thermocline depth and temperature, whereas the center of gravity of the subsurface cyanobacteria biovolume scales linearly with the mixed layer depth and temperature. Furthermore, our data suggest there is a seasonal evolution of the subsurface cyanobacteria center of gravity that could potentially indicate timing of HAB onset. Based on easily measured parameters associated with the vertical lake temperature profile and meteorological conditions, we provide evidence of predictable trends in subsurface cyanobacteria variables.

1 **Abiotic drivers of a deep cyanobacteria layer in a**
2 **stratified and eutrophic lake**

3 **J. Taylor^{1,2}, M. Hondzo^{1,2}, and V. R. Voller^{1,2}**

4 ¹University of Minnesota, Twin Cities – Department of Civil, Environmental, and Geo-Engineering

5 ²University of Minnesota, Twin Cities – St. Anthony Falls Laboratory

6 **Key Points:**

- 7 • In a eutrophic and stratified lake environment, magnitude of subsurface cyanobacteria
8 peak concentration is driven primarily by thermocline depth and temperature
9 • In a eutrophic and stratified lake environment, center of gravity of subsurface cyanobac-
10 terial biomass is driven primarily by surface layer depth and temperature

Corresponding author: J. Taylor, tay11562@umn.edu

Abstract

Harmful algal blooms (HABs), in particular those consisting of the cyanobacteria *Microcystis*, are becoming increasingly more common across the globe. Despite the growing body of evidence that suggests vertical heterogeneity of *Microcystis* can be a precursor to HAB formation, the abiotic drivers of vertical distribution of *Microcystis* are poorly understood in the field environment. The prediction of subsurface cyanobacteria is also pertinent because subsurface concentrations are not easily recognizable to the public or lake system managers, creating an unnoticed safety hazard. High-frequency temporal and vertical data were collected from an Eulerian research station anchored in a stratified and eutrophic lake for five months. Data show that the magnitude of the subsurface *Microcystis* concentration peak and the center of gravity of the deep cyanobacteria layer are statistically significantly mediated by the thermal structure of the lake. The peak subsurface cyanobacteria biovolume scales linearly with the thermocline depth and temperature, whereas the center of gravity of the subsurface cyanobacteria biovolume scales linearly with the mixed layer depth and temperature. Furthermore, our data suggest there is a seasonal evolution of the subsurface cyanobacteria center of gravity that could potentially indicate timing of HAB onset. Based on easily measured parameters associated with the vertical lake temperature profile and meteorological conditions, we provide evidence of predictable trends in subsurface cyanobacteria variables.

1 Introduction

Harmful algal blooms are one of the most imminent threats to freshwater quality across the globe (O’Neil et al., 2012; Huisman et al., 2018). Of the HAB-forming cyanobacteria species, *Microcystis* are of particular concern due to their ubiquity and their production of Microcystin toxins. There are numerous evolutionary advantages that allow *Microcystis* to thrive across the globe, and one such advantage in stratified lakes is the ability of vertical motility. Cell buoyancy is modulated by adjusting ballast weight through production or metabolism of dense carbohydrates to offset low density intracellular gas vesicles, *Microcystis* are able to move up or down the water column (Reynolds et al., 1987). The speed of unicellular vertical motility can be greatly enhanced by forming colonies, which is a typical occurrence in natural environments (Xiao et al., 2018).

Traditionally, *Microcystis* vertical migration in natural environments has been hypothesized to be nutrient-driven chemotaxis (Fogg & Walsby, 1971; Ganf & Oliver, 1982). However, as lakes become more eutrophic and nutrients become a less limiting substrate, abiotic factors tend to dominate *Microcystis* vertical motility (Xiao et al., 2018). Most of the work on abiotic drivers has focused on light, wind, and temperature. Thomas and Walsby (1985, 1986) demonstrated experimentally that *Microcystis* cells will increase in density under high irradiance conditions to sink to a preferred low light intensity, but their ability to regain buoyancy was dependent on water temperature. Cao et al. (2006) suggested vertical distributions of different phytoplankton species, especially *Microcystis*, were largely correlated with wind events (and had no correlation with nutrients) in a field study of Lake Taihu, China. As a result, it has been suggested the relationship between *Microcystis* vertical motility and timing of HAB onset should be explored more in depth (Xiao et al., 2018; Zhu et al., 2018; Liu et al., 2019). There have been several models formulated to simulate *Microcystis* vertical motility as a function of abiotic factors (Wallace et al., 2000; Medrano et al., 2013; Zhu et al., 2018), and Yao et al. (2017) connected their simulations of *Microcystis* motility to a hypothesis of necessary conditions for bloom formation, but none have had a long-term, high-frequency, *in situ* temporal data set for validation.

Aside from being active movers, *Micrycosystis* can also act as passive particles in a water column. Field investigations including Bormans et al. (1999) suggest surface dynamics play the largest role in determining vertical distribution of *Microcystis*. Marti et al. (2016) used relevant time scales of vertical transport in the surface layer and the metal-

62 innion, vertical mixing in the surface layer and the metalimnion, and vertical migration of
63 cyanobacteria to characterize when algae were acting as free movers or passive particles. It
64 was suggested, through field work and 3-D simulations, that the time-scale hierarchy—how
65 fast one process happens compared to another—determines success of particular algal species
66 at specific locations in the lake. A field study by Hozumi et al. (2019) demonstrated that
67 low turbulence levels in the surface layer of Lake Kinneret, Israel led to a thin, dense *Micro-*
68 *cystis* scum layer, while higher levels of turbulence led to a thick, sparse *Microcystis* layer.
69 These findings were corroborated in a mesocosm experiment conducted by X. Wu et al.
70 (2019). To further complicate the relationship between lake hydrodynamics and cyanobac-
71 teria, Sommer et al. (2017) demonstrated that dense layers of motile algae can create a great
72 enough density instability to modulate the mixed layer depth, as corroborated by the field
73 study conducted by Sepúlveda Steiner et al. (2019).

74 The phenomenon of subsurface peaks in cyanobacterial biomass concentration has been
75 studied extensively in both ocean and lake environments. This feature is often referred to as
76 a deep chlorophyll maximum, or DCM (Cullen, 1982), and the zone in which this increase
77 in biomass occurs is called a deep chlorophyll layer, or DCL (Brooks & Torke, 1977). The
78 abiotic drivers of DCL formation have been extensively studied (Cullen, 2015). Huisman
79 et al. (2006) demonstrated through numerical simulations that there exists a minimum
80 turbulence level in the surface layer of the ocean in order to achieve a stable DCM. Scofield et
81 al. (2017) conducted a field study on Lake Ontario and determined significant dependencies
82 of DCM magnitude and location on the temperature profile of a lake; Sanful et al. (2017)
83 demonstrated euphotic depth was the primary driver of DCM formation and maintenance
84 in another field study. Somavilla et al. (2019) connected deep chlorophyll phenomena to
85 surface blooms in an oceanic environment: field data demonstrated that cyanobacterial
86 biomass was prevalent below the diurnal mixed layer, towards a DCL, when the net heat
87 flux at the water surface became positive on a seasonal timescale. Lastly, despite being a
88 major topic of study for four decades, the actual definition of a DCL or DCM is largely
89 ambiguous. How deep is "deep"? What is the depth of the maximum biomass for profiles
90 with two or more peaks in the DCL? Xu et al. (2019) developed a robust machine learning
91 algorithm to help unify these definitions, but perhaps the problem is in the parameters we
92 are defining than in how we define them.

93 The work highlighted above has brought many interesting insights to the field. How-
94 ever, as is almost always the case when dealing with microorganisms, discrepancies exist
95 between experiments with short-term, high-frequency observations and field data with long-
96 term, low-frequency observations. Further, DCM and DCL definitions and parameters (or
97 lack thereof) make it difficult to draw cohesive conclusions between studies. To bridge
98 these gaps, we anchored a research station from May to August of 2017 in a stratified and
99 eutrophic lake with a history of *Microcystis* blooms. This research station recorded mete-
100 orological and water temperature conditions every five minutes and water quality variables
101 every two hours. Data were then used to inform and validate a stepwise regression model
102 to determine the relationship between the light, wind speed, and temperature profiles of a
103 lake with the magnitude and shape of a deep cyanobacteria layer (DCL from here on out), a
104 potential precursor to a harmful algal bloom. Formal definitions and a new shape parameter
105 for the DCL were introduced, as well as a potential method for predicting bloom formation
106 when a DCL is present.

107 2 Methods

108 2.1 Field site

109 South Center Lake, Fig. 1a, is a eutrophic and dimictic lake in Chisago County, MN
110 that stratifies from May to October. It has a surface area of approximately 3.3 km², a max-
111 imum depth of 33 m, an average depth of nearly 5 m, and its shoreline is mostly developed.
112 Due to its status as a Minnesota Pollution Control Agency (MPCA) Sentinel lake, South

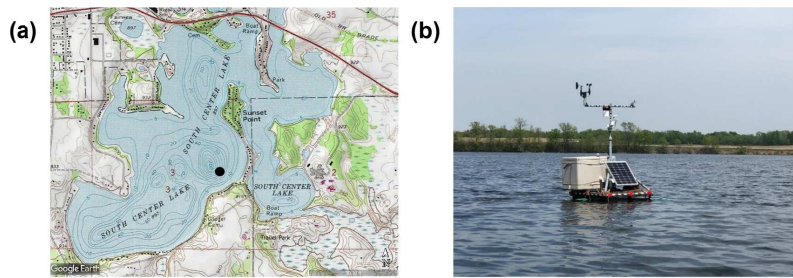


Figure 1: (a) USGS contour map of South Center Lake. Black dot indicates position of research station. (b) Research station.

113 Center Lake has a wealth of historical data, with the first lake survey occurring in 1942 and
 114 regular water quality data from 1997 to present day. This historical data, which indicates
 115 a reoccurring summer-time *Microcystis* bloom, was used to supplement measurements from
 116 our research station (Engel et al., 2011). For instance, historic phytoplankton assemblages
 117 indicate South Center Lake, in a location near where our measurements were taken, is al-
 118 most entirely cyanobacteria dominant year-round, besides some diatoms and green algae
 119 in early summer. MPCA data were also used to corroborate grab sample measurements,
 120 detailed in Section 2.3.

121 2.2 Research station

122 The research station was anchored in South Center Lake from May 12, 2017 to Octo-
 123 ber 30, 2017 (Fig. 1b). The data used in analysis extends to September 3rd, 2017—the end
 124 of *Microcystis* domination (Wilkinson et al., 2020). The lake depth was 14 m deep at the
 125 location of the water station. The research station records meteorological measurements—
 126 wind speed, wind direction, air temperature, relative humidity, photosynthetically active
 127 radiation (PAR), and rain depth—every five minutes. In addition, a thermistor chain records
 128 water temperature at depths of 0.1, 1, 2, 3, 4, 5, 6, 7, 8, 10, 12, and 14 m every five min-
 129 utes. The water quality profiler takes measurements of dissolved oxygen concentration, pH,
 130 phycocyanin concentration, PAR, specific conductivity, and water temperature at depths of
 131 1, 1.5, 2, 2.5, 3, 3.5, 4, 4.5, 5, 6, 7, 8, 9, 10, 11, 12, 13, and 14 m every two hours. For
 132 a full description of equipment used, see Wilkinson et al. (2020). An example profile for
 133 temperature, biovolume, and PAR is shown in Fig. 2.

134 2.3 Data analysis

135 Water column parameters that describe the vertical thermal structure of the lake were
 136 determined from the Lake Analyzer and Lake Heat Flux Analyzer software in Matlab (Read
 137 et al., 2011; Woolway et al., 2015). Weekly grab samples were taken to measure nutrient,
 138 phycocyanin, and estimate biovolume concentrations throughout the water column. The *in*
 139 *situ* field measurements of phycocyanin, a protein found only in cyanobacteria, was linearly
 140 regressed to the laboratory measurements of the corresponding phycocyanin grab samples
 141 and the *Microcystis* biovolume estimates (Wilkinson et al., 2020).

142 The average mode-1 vertical seiche period of South Center Lake estimated from the
 143 Lake Analyzer software was approximately four hours. Water temperature and research
 144 station data were averaged over this seiche period to determine diurnal and seasonal trends.
 145 The mixed layer depth, h_{ML} , was defined as the first depth with a temperature difference of
 146 at least -0.3°C from the surface water temperature. The thermocline depth, h_T , was defined
 147 as the depth at which the maximum temperature gradient occurs. The euphotic depth,
 148 h_{EP} was defined as the depth at which PAR intensity was 1% of the PAR intensity of the

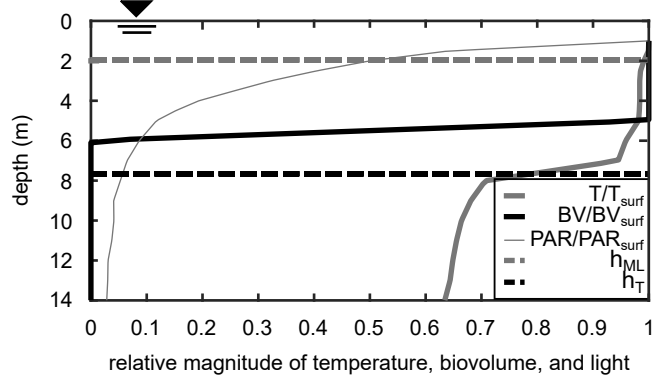


Figure 2: Profile from 24 May, 2017 6:02pm of normalized temperature (thick solid gray line), biovolume (thick solid black line), and light (thin solid gray line) profile generated from research station profiler data. Mixed layer depth (horizontal dashed gray line) and thermocline depth (horizontal dashed black line) also shown. Water surface is at 0 m, and the lake bed is at 14 m. Here, $T_{surf} = 14.77^{\circ}\text{C}$, $BV_{surf} = 2.76 \times 10^6 \mu\text{m}^3/\text{mL}$, and $\text{PAR}_{surf} = 166.3 \mu\text{mol/s/m}^2$.

149 water surface. Mixed layer temperature, T_{ML} , was then defined as the water temperature
 150 at the mixed layer depth, with corresponding definitions for the thermocline temperature,
 151 T_T , and the euphotic temperature, T_{EP} . The thermocline steepness, m_T , was defined as
 152 the temperature gradient at the thermocline. Since research station data were recorded at
 153 discrete depths (Sec. 2.2), a piecewise linearly interpolated line was fitted to research station
 154 profiler data to create pseudo-continuous profiles. For the convenience of the reader, key
 155 parameters derived from measurements along with appropriate scalings are given in Table
 156 1.

Table 1: Relevant temperature profile parameters^a

parameter	variable	comment
mixed layer depth	\tilde{h}_{ML}	depth of base of surfaced mixed layer
thermocline depth	\tilde{h}_T	depth of maximum magnitude temperature gradient
euphotic depth	\tilde{h}_{EP}	depth where PAR reaches 1% of surface PAR
mixed layer temperature	\tilde{T}_{ML}	water temperature at mixed layer depth
thermocline temperature	\tilde{T}_T	water temperature at thermocline depth
euphotic temperature	\tilde{T}_{EP}	water temperature at euphotic depth
thermocline steepness	\tilde{m}_T	temperature gradient at the thermocline depth

^a Parameters have been made dimensionless, as indicated by the tilde. All depths were normalized by dividing by $h_{max} = 14\text{m}$, the maximum depth of the water column at the location of the research station. All temperature were normalized by multiplying by α , the coefficient of thermal expansion ($^{\circ}\text{C}$). The thermocline steepness was normalized by multiplying by αh_{max} .

157

2.4 Deep cyanobacteria layer definitions

158

159

160

161

162

163

164

165

166

167

168

169

170

A deep cyanobacteria layer (DCL) is defined to be present if there exists a biovolume concentration, C , below the diurnal mixed layer depth that is greater than the maximum concentration within the diurnal mixed layer (Fig. 3). If this condition is met, then the top of the DCL, z_{TOP} , is defined as the first depth of increasing phycocyanin concentration below the mixed layer. The bottom of the DCL, z_{BOT} , is defined as the first depth after z_{TOP} such that the phycocyanin concentration goes below the average concentration within the mixed layer. The dimensionless center of gravity of the DCL, z_{CG} , can then be defined as

$$z_{CG} = \frac{1}{h_{max}} \left(\frac{\int_{z_{BOT}}^{z_{TOP}} zC dz}{\int_{z_{BOT}}^{z_{TOP}} C dz} \right) \quad (1)$$

where h_{max} is the maximum depth of the water column at the location of the research station ($h_{max} = 14\text{m}$). Dividing by h_{max} ensures not only that z_{CG} is dimensionless, but also that it is scaled from 0 to 1, from the water surface to the lake bed, respectively (Fig. 4).

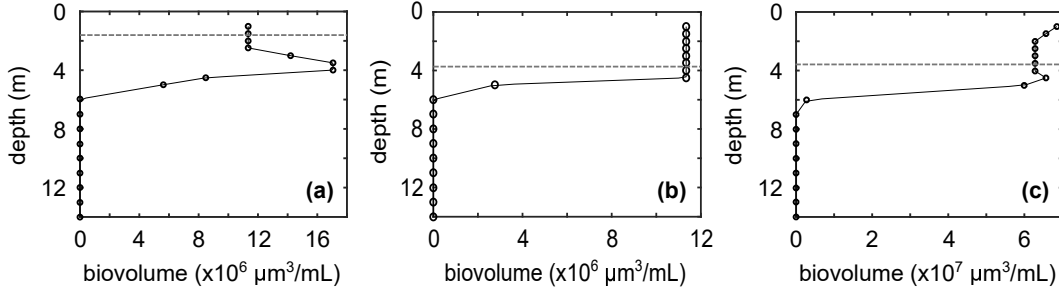


Figure 3: Example biovolume profiles when (a) a DCL is present (July 4th, 2017 18:00), (b) a uniform biovolume distribution with no DCL present (July 13th, 2017 04:00), and (c) a surface biovolume peak with no DCL present (August 4th, 2017 16:00). Thin black lines with open circle markers indicate the biovolume profile, and horizontal dashed grey lines indicate the mixed layer depth. Note that in (c), although there is an increase in biovolume below the mixed layer depth, it is not significantly large enough compared to the average concentration within the mixed layer to be considered a DCL.

171

172

173

174

175

176

C_{DCL} is a dimensionless variable that describes the relative magnitude of the DCL peak biovolume concentration to the biovolume concentration within the mixed layer and is defined as follows:

$$C_{DCL} = \frac{C_{DCL,max} - C_{ML,avg}}{C_{ML,avg}} \quad (2)$$

where $C_{DCL,max}$ is the maximum biovolume concentration within the DCL and $C_{ML,avg}$ is the average biovolume concentration in the mixed layer.

177

2.5 Modeling DCL variables

178

179

180

181

182

183

184

We can ensure DCL definitions are physically meaningful if we can predict them with relevant forcings. Under low nitrogen to phosphorus ratio conditions, which is preferred by *Microcystis* (Fujimoto et al., 1997; Wurtsbaugh et al., 2019), it is hypothesized that the characteristics of the DCL are controlled by the vertical temperature structure and light conditions in the lake. That is, if a DCL is present, its center of gravity and magnitude can be expressed as functions of the variables in Table 1 to arrive at the following:

$$z_{CG} = f(\tilde{h}_{ML}, \tilde{h}_T, \tilde{h}_{EP}, \tilde{T}_{ML}, \tilde{T}_T, \tilde{T}_{EP}, \tilde{m}_T) \quad (3)$$

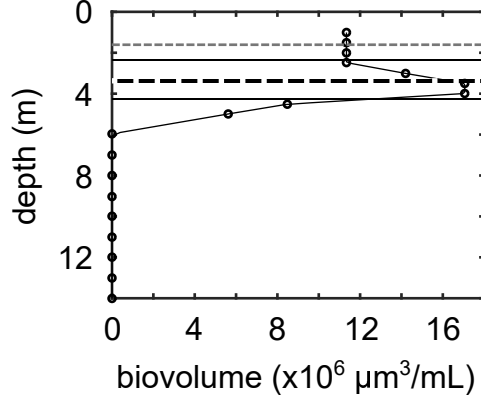


Figure 4: Example biovolume profile with a DCL (July 4th, 2017 18:00, Fig. 3a). Thin black line with open circle markers indicate the biovolume profile, horizontal dashed gray line indicated the mixed layer depth, horizontal solid black lines indicate the bounds of the DCL, and horizontal dashed black line indicates the DCL center of gravity.

185
186

$$C_{DCL} = g(\tilde{h}_{ML}, \tilde{h}_T, \tilde{h}_{EP}, \tilde{T}_{ML}, \tilde{T}_T, \tilde{T}_{EP}, \tilde{m}_T) \quad (4)$$

187
188
189
190
191
192
193
194
195
196
197

A regression analysis was performed to determine what physical parameters and interactions of physical parameters had the most significant impact on the normalized maximum biovolume concentration in the DCL, C_{DCL} , and the normalized center of gravity of biovolume in the DCL, z_{CG} . Matlab’s Statistical and Machine Learning Toolbox and, in particular, the Matlab function `stepwiselm` was used. Daytime profiles were separated from nighttime profiles to determine the impact of the light regime on the DCL characteristics. In the analysis of the nighttime profiles, variables \tilde{T}_{EP} and \tilde{h}_{EP} were dropped. A model that includes both linear and bi-linear (interaction) terms was then generated to predict $C_{DCL,all}$, $C_{DCL,day}$, $C_{DCL,night}$, $z_{CG,all}$, $z_{CG,day}$, and $z_{CG,night}$. Once full models had been derived, observational trends were used to create parsimonious models with the lowest number of parameters that were still able to explain the data variability with statistical significance.

198

3 Results

199
200

3.1 Seasonal trends of water temperature, biological, and meteorological data

201
202
203
204
205
206
207
208
209
210

The temperature and biovolume profiles depicted seasonal and vertical patterns of thermal stratification and cyanobacterial accrual from June to October 2017 (Fig. 5). Temperature stratification over the lake depth was established before June 2017 and the lake experienced thermal structure overturn shortly before November. Significant subsurface peaks in biovolume appeared at the beginning of June and July, and a surface bloom formed in early August. Grab samples show *Microcystis* was the dominant biovolume genera up until the surface bloom in early August when *Planktothrix* began to dominate the composition of cyanobacteria (Wilkinson et al., 2020). For the remainder of the analysis, we will focus only on the period of stratification from June to October, with a particular emphasis from June until the harmful algal bloom in early August when *Microcystis* was dominant.

211
212
213
214

Time series of wind speed and air-water temperature difference are included to provide a sense of the meteorological forcings of the thermal and algal structure of the lake (Fig. 6). Overall, surface water temperatures were higher than the air temperatures, thereby indicating prevalence of natural cooling due to the heat loss from the surface mixed layer

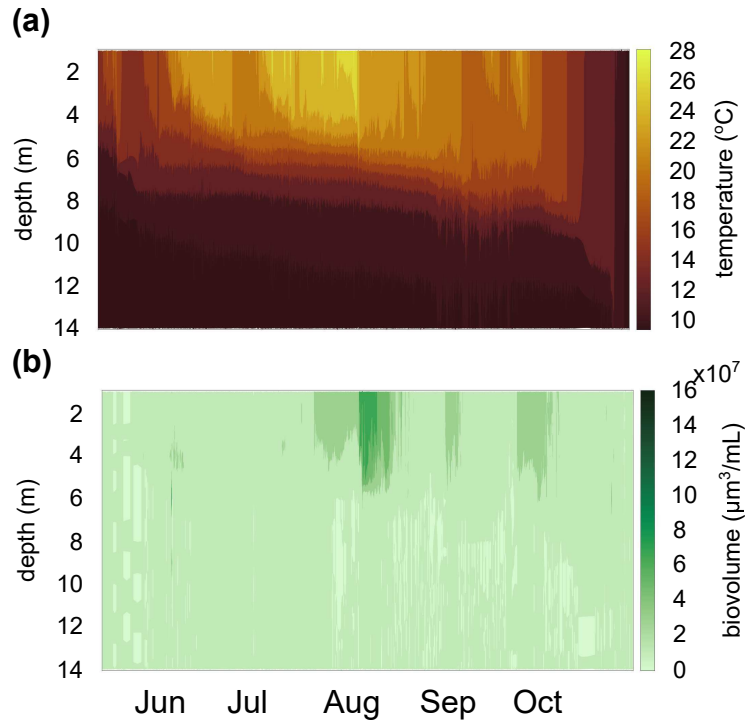


Figure 5: (a) Temperature contours and (b) biovolume contours at the location of the research station over the entire observation period. Air-water interface is at 0m.

215 (Fig. 6b) The seasonal trend of four important water column depths: the mixed layer
 216 depth (h_{ML}), the center of gravity of the DCL biovolume (z_{CG}), the thermocline depth
 217 (h_T), and the euphotic depth (h_{EP}) are depicted in Fig. 6c. The euphotic depth was
 218 essentially always well below the thermocline depth. The relative magnitude of the peak
 219 DCL biovolume concentration increases for a significant period of time in early June and
 220 early July (Fig. 6d). The data demonstrate that a deep cyanobacteria layer is associated
 221 with low wind speeds and air temperatures warmer than surface water temperatures. Both
 222 subsurface peaks eventually disperse, and do not form surface blooms.

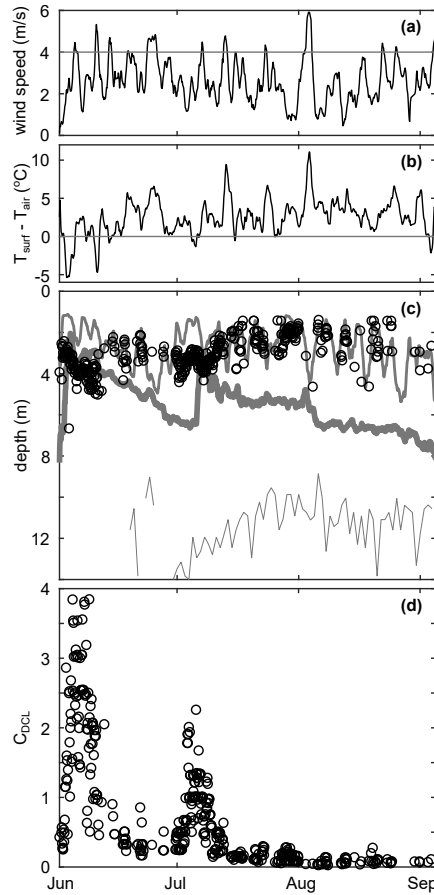


Figure 6: Time series of (a) wind speed (thin horizontal grey line indicates wind speed of 4 m/s), (b) $T_{surf} - T_{air}$ (thin horizontal grey line indicates a temperature difference of zero), (c) important depth (mixed layer depth as the medium thickness grey line, thermocline depth as the thick grey line, euphotic depth as the thin grey line, and center of gravity of the DCL—as calculated by Eqn. 1—as the open black circles), and (d) relative peak magnitude of the DCL biovolume. There are two periods with significantly large C_{DCL} values: June 1st – June 13th and July 1st - July 9th. Air-water interface is at 0 m. Data was smoothed over a 24-hour window in order to clearly show long-term trends, with the exception of z_{CG} and C_{DCL} , which were left as calculated.

223 Comparing biovolume concentration profiles to temperature profiles seems to suggest
 224 a relationship between the stability of the thermal structure and vertical heterogeneity of
 225 the vertical biovolume distribution (Fig. 7). Profiles with a well-defined and deep uniform
 226 surface layer and metalimnion are associated with biovolume profiles with all the biomass
 227 concentrated in a uniform surface layer (Fig. 7a and 7b). Thermal profiles with a well-
 228 defined and shallow uniform surface layer but a terraced metalimnion are associated with
 229 biovolume profiles with deep cyanobacteria layers (Fig. 7c and 7d). Lastly, thermal profiles
 230 with a not well-defined surface layer are associated with biovolume profiles with surface (or
 231 near-surface) peaks (Fig. 7e and 7f). Eqns. 1 and 2 appear to appropriately characterize
 232 cyanobacterial vertical heterogeneity (see Appendix Appendix A for further discussion).

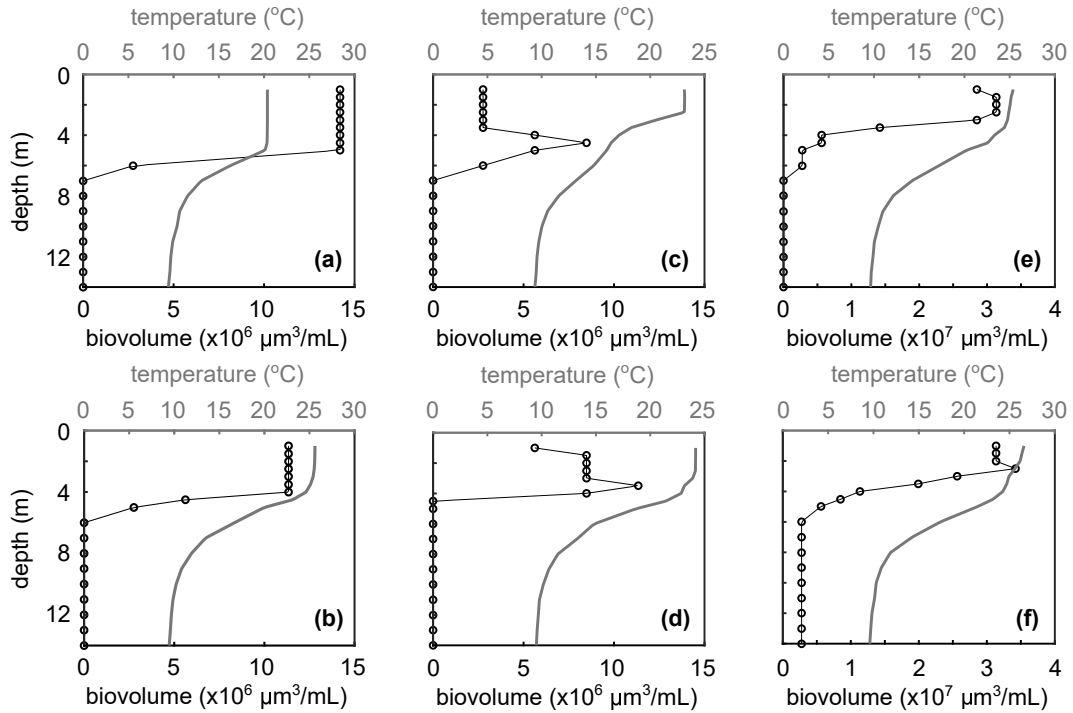


Figure 7: Example profiles taken (a) June 30, 2017 08:00, (b) July 13, 2017 02:00, (c) June 9, 2017 06:00, (d) June 17, 2017 20:00, (e) July 21, 2017 16:00, and (f) July 30, 2017 20:00. Thin black lines with open circle markers indicate biovolume concentration (bottom axis) and solid gray lines indicate temperature (top axis). (a) and (b) are examples of profiles with a uniform biovolume profile, (c) and (d) are examples of profiles with a deep cyanobacteria layer, and (e) and (f) are examples of profiles with a near-surface biovolume peak.

233

3.2 DCL Modeling results

234

235

236

237

238

239

Since nutrient conditions did not appear to be a significant driver of cyanobacterial vertical heterogeneity throughout the observation period of South Center Lake (Appendix Appendix B), the protocol outlined in Sec. 2.5 was used to fit models to C_{DCL} and z_{CG} (Table 2). The euphotic depth was deeper than the DCL for most of the observation period, so there was an insignificant difference between daytime and nighttime biovolume profile behavior, and only results for all profiles are shown.

Table 2: Stepwise regression results

DCL variable	parameter	coefficient estimate
a) z_{CG}, all profiles		
n = 417, $r^2 = 0.66$, RMSE = 0.034 ($0.099 \leq z_{CG} \leq 0.48$)		
	intercept	-0.23
	\tilde{h}_{ML}	0.21
	\tilde{h}_T	0.71
	\tilde{T}_{ML}	110
	\tilde{T}_T	65
	$\tilde{h}_{ML}\tilde{h}_T$	1.0
	$\tilde{h}_T\tilde{T}_{ML}$	-190
	$\tilde{h}_T\tilde{T}_T$	-77
	$\tilde{T}_{ML}\tilde{T}_T$	-12000
b) C_{DCL}, all profiles		
n = 417, $r^2 = 0.65$, RMSE = 0.52 ($0.027 \leq C_{DCL} \leq 3.8$)		
	intercept	0.33
	\tilde{h}_T	0.90
	\tilde{T}_{ML}	1300
	\tilde{T}_T	-970
	\tilde{m}_T	-190
	$\tilde{h}_T\tilde{T}_{ML}$	-2000
	$\tilde{T}_{ML}\tilde{m}_T$	44000
	$\tilde{T}_T\tilde{m}_T$	-18000

Stepwise regression results for **(a)** the center of gravity of the DCL biovolume and **(b)** the relative peak magnitude of the DCL biovolume. Full regression parameters listed in Table 1, although euphotic depth parameters were excluded since the euphotic depth was well below the thermocline for much of the observation period. The coefficient estimate column gives estimates of coefficients, and bolded p-values are those under the threshold of 0.05.

240 While the models outlined in Table 2 can predict values of C_{DCL} and z_{CG} to a relatively
 241 high degree, the models are rather cumbersome and difficult to assign physical meaning
 242 to. In an effort to achieve conceptually sound models that retain statistical significance,
 243 parsimonious models were generated using the full stepwise regression results as a first
 244 iteration and observational data as guides. Upon inspection of Fig. 6c and 6d, the difference
 245 in peak magnitude between the June and July peaky periods could be due to the difference
 246 in thermocline depth: a deeper thermocline depth in July seems to have led to a lower
 247 magnitude relative peak. Further, location of the DCL center of gravity seems to be related
 248 to the mixed layer depth (see also Fig. 7). Using these observations, input parameters from
 249 Tables 1 and 2 were stripped to just \tilde{h}_T and \tilde{T}_T for predicting C_{DCL} and \tilde{h}_{ML} and \tilde{T}_{ML} for
 250 predicting z_{CG} . These reduced complexity inputs generated the following expressions:

$$251 \quad z_{CG} = 0.27 + 0.61\tilde{h}_{ML} - 22\tilde{T}_{ML} \quad (5)$$

252 which explains the data (n = 417 profiles) with an r^2 of 0.42 and a root-mean-squared error
 253 (RMSE) of 0.044. Eqn. 4 reduces to

$$254 \quad C_{DCL} = 5.6 - 8.2\tilde{h}_T - 530\tilde{T}_T \quad (6)$$

255 which explains the data ($n = 417$ profiles) with an r^2 value of 0.57 and an RMSE of 0.57.
 256 These parsimonious models reduce input parameters to two while maintaining a large portion
 257 of the statistical significance (Fig. 8).

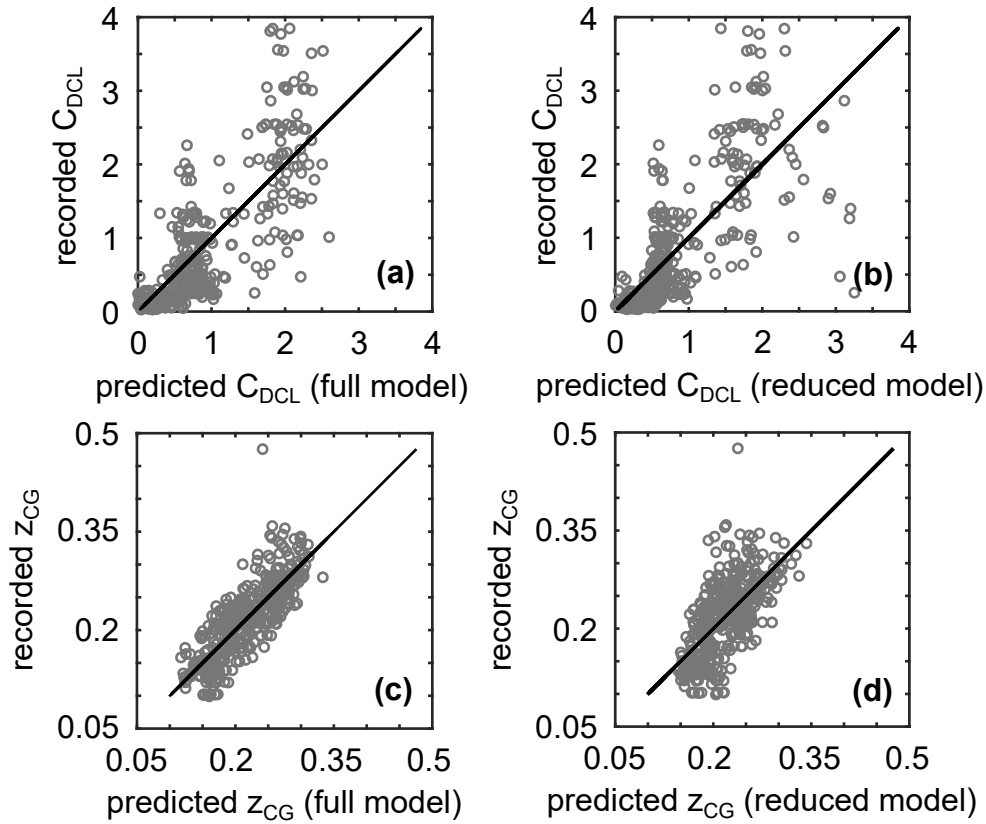


Figure 8: Goodness-of-fit results for models of (a) C_{DCL} using full stepwise regression results in Table 2b, ($n = 417$, $r^2 = 0.65$, $RMSE = 0.52$), (b) C_{DCL} using the simplified Eqn. 6 ($n = 417$, $r^2 = 0.57$, $RMSE = 0.57$), (c) z_{CG} using full stepwise regression results in Table 2a ($n = 417$, $r^2 = 0.66$, $RMSE = 0.034$), and (d) z_{CG} using the simplified Eqn. 5 ($n = 417$, $r^2 = 0.42$, $RMSE = 0.044$). Solid black lines show a one-to-one line.

258 4 Discussion

259 4.1 DCL behavior

260 Stepwise regression results indicate the center of gravity of the DCL biovolume is
 261 controlled by mixed layer depth and temperature (Eqn. 5), whereas the magnitude of the
 262 DCL biovolume peak is controlled by thermocline depth and temperature (Eqn. 6). Because
 263 *Microcystis* moves up and down a water column by adjusting cell density, we expect the
 264 thermocline depth—the depth of the largest magnitude density gradient—to act as a boundary
 265 condition. Not necessarily impenetrable (see early June period in Fig. 6c where the center of
 266 gravity of the DCL is actually below the thermocline depth), but more like a discontinuous
 267 step change from high to low diffusivity. Therefore, as the thermocline deepens, the width
 268 of habitable space for the algae increases. In this situation, we would expect the algae
 269 to diffuse throughout the entire habitable space, thereby decreasing peakiness. Following
 270 similar logic, increasing the temperature at the thermocline depth would also increase this
 271 habitable space, since temperature is monotonically decreasing and algae like it hot (Paerl

272 & Huisman, 2008), so we would again expect a more diffuse and less peaky distribution of
273 algae.

274 Next, since well-mixed conditions will likely impede algal aggregation, we expect the
275 center of gravity to deepen as the mixed layer depth deepens. Conversely, as a result of
276 thermotaxis towards a preferred high temperature (water temperatures at the mixed layer
277 never reached lethal conditions, as can be seen in Fig. 5a), we would expect the center of
278 gravity to move shallower as the temperature at the mixed layer increases. This can be
279 thought of as a balance between hydrodynamic forcings and biological preferences.

280 Eqns. 5 and 6 predict recorded values of C_{DCL} and z_{CG} to a reasonable accuracy
281 with statistical significance for all profiles (Fig. 8). Given a temperature profile, Eqns. 5
282 and 6 will output DCL relative peak magnitude and center of gravity. Lakes are complex
283 ecosystems, and cyanobacteria are remarkably sensitive to all different kinds of forcings,
284 hydrodynamic and biological alike. However, it seems that a significant portion of the
285 hydrodynamic dependencies can be packaged into thermal structure parameters that are
286 relatively easy to measure. Further, in the stratified and eutrophic conditions seen through-
287 out the observation period, biological forcings, which are difficult and time-consuming to
288 measure, are secondary controls of the vertical distribution of cyanobacterial biomass.

289 It's prudent to note that these modeling results only make sense for the range of input
290 variables given. For example, if the temperature in the mixed layer ever got too hot to
291 be lethal to algae, any increase in temperature would likely lead to algae moving to cooler
292 temperatures at deeper depths in the water column, and the DCL center of gravity would
293 increase. However, the hottest water temperatures recorded at South Center Lake over the
294 summer of 2017 was approximately 28°C, which is right around the ideal temperature for
295 *Microcystis*. Further, if the euphotic depth had not been below the thermocline for almost
296 the entirety of the observation period, it is likely the euphotic depth would have had a
297 statistically significant relationship with both C_{DCL} and z_{CG} . Lastly, nutrient conditions
298 were favorable for *Microcystis* throughout the duration of the observation period (Appendix
299 Appendix B). If the algae had to search for appropriate nutrient levels, this could negatively
300 impact the accuracy of predictions.

301 4.2 DCL formation

302 Observational data suggest deep cyanobacteria layers are formed during periods of
303 little to no wind shearing and natural convection (Fig. 6a and 6b). Results suggest that
304 the location of the DCL center of gravity is determined by the mixed layer depth and the
305 temperature at the mixed layer depth. To determine the role of wind shearing and natural
306 convection, the penetrative convective velocity is introduced as

$$307 w_* = (Bh_{ML})^{\frac{1}{3}} \quad (7)$$

308 where B is the buoyancy flux in m^2/s^3 (Imberger, 1985). If we assume the air-water tem-
309 perature difference is the dominant heat flux term, we can define the buoyancy flux at the
310 water surface as

$$311 B = \frac{g\alpha}{\rho C_P} H_Q$$

$$\approx \frac{g\alpha}{\rho C_P} \left(k \frac{\partial T}{\partial z} \right)_{z=0} \quad (8)$$

$$\approx \frac{g\alpha}{\rho C_P} \left(k \frac{T_{surf} - T_{air}}{\delta_t} \right)$$

312 where g is the gravitational acceleration (m/s^2), α is the coefficient of thermal expansion
313 ($1/K$), ρ is the water density (kg/m^3), C_P is the specific heat of water ($J/kg/K$), H_Q is
314 the total heat flux at the water surface (W/m^2), k is the thermal conductivity of water

315 (W/m/K), and taking $T_{surf} \approx T_{ML}$ by assuming an infinitely small air-side boundary
 316 layer. A positive buoyancy flux, then, indicates the lake is undergoing surface cooling.
 317 J. Wu (1971) provides an estimation for δ_t , the thermal diffusivity layer thickness (m), to
 318 be

$$319 \quad \delta_t = 5.5 \frac{\nu}{u_*} \quad (9)$$

320 where ν is the kinematic viscosity of water (m^2/s) and u_* is the shear velocity at the water
 321 surface (m/s). We can now introduce a Reynolds number for penetrative convection at the
 322 water surface to be

$$323 \quad Re = \frac{w_* h_{ML}}{\nu} \\ = \frac{(Bh_{ML})^{\frac{1}{3}} h_{ML}}{\nu}$$

324 Hence,

$$325 \quad Re = \frac{(g\alpha D_T (T_{ML} - T_{surf}))^{\frac{1}{3}} h_{ML}}{\nu} \quad (10)$$

326 where $D_T = \frac{kh_{ML}}{\rho C_P \delta_t}$ is the thermal dispersion coefficient. Using this formulation for a
 327 Reynolds number relevant to surface thermal cooling, profiles undergoing conditions such
 328 that $Re > 5 \times 10^4$ virtually never formed a DCL for the entirety of the observation period
 (Fig. 9).

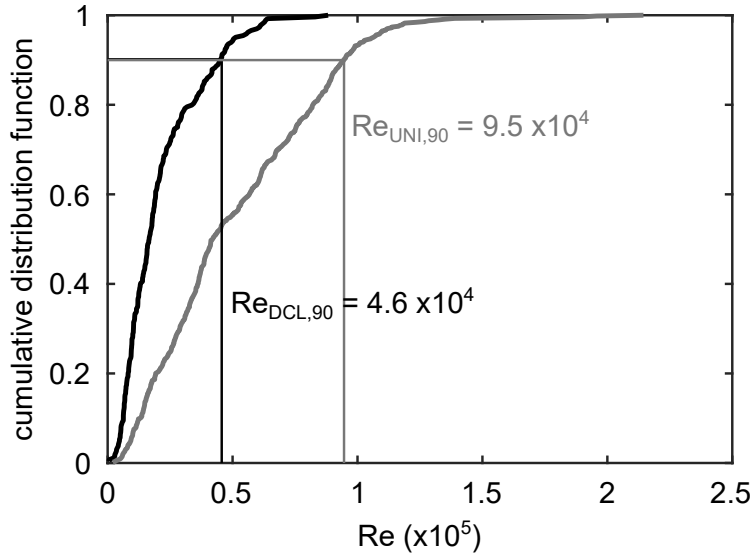


Figure 9: Surface thermal cooling Reynolds number cumulative distribution function (CDF). Black line is the CDF for profiles with a DCL, gray line is the CDF for profiles without a DCL. 90% of profiles with a DCL have concurrent Re values of 4.6×10^4 or less; 90% of profiles without a DCL have concurrent Re values of 9.5×10^4 or less.

329

330 Eqn. 10 states that $Re \sim h_{ML}(T_{surf} - T_{air})^{\frac{1}{3}}$. These results reveal two important
 331 points. The first is that the deeper the mixed layer depth, the less likely it is that a DCL
 332 will form (Fig. 10a and 10b). In fact, the two situations seem to have two entirely different
 333 distributions of mixed layer depths: profiles with a DCL follow a power law, whereas profiles
 334 without a DCL follow a uniform distribution. Since the euphotic depth was well below the
 335 thermocline for the entirety of the observation period (Fig. 6c), light was not limiting the

336 aggregation of *Microcystis* below the mixed layer depth. The lack of a DCL, then, is likely
 337 due to the physical drivers, like wind shearing (Pollard et al., 1972; Ushijima & Yoshikawa,
 338 2020), of a deepening mixed layer depth. Secondly, from Eqn. 10, we can also infer that
 339 the greater the surface water temperature is relative to the air temperature, the less likely
 340 it is that a DCL will form (Fig. 10c and 10d). The temperature difference ($T_{surf} > T_{air}$)
 341 promotes natural convection-induced turbulence at the water surface. In effect, the data
 342 indicate the likelihood of a DCL occurring decreases as surface layer processes like wind
 343 shearing and natural convection increase.

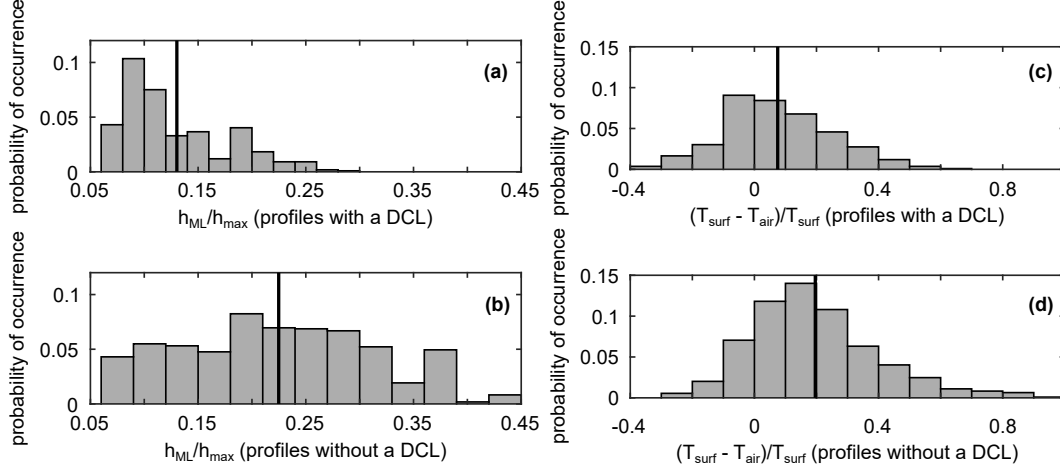


Figure 10: Histograms of (a) normalized mixed layer depth for profiles with a DCL, (b) normalized mixed layer depth for profiles without a DCL, (c) normalized air-water temperature difference for profiles with a DCL, and (d) normalized air-water temperature difference for profiles without a DCL. Vertical lines indicate mean values of (a) 0.13, (b) 0.22, (c) 0.076, and (d) 0.19.

344

4.3 DCL fate

345

346

347

348

349

350

After formation and behavior of the deep cyanobacteria layer comes its fate: Does it disperse and form a uniform algae profile, or does it form a surface bloom? Both the June and July DCLs develop large peaks, although the June DCL center of gravity travels much deeper than the July. Water temperatures in the surface layer are high enough to sustain cyanobacterial life, nutrient conditions are sufficient, and yet neither subsurface peaks form a surface bloom. To address this, we introduce a new term, ζ defined as

351

$$\zeta = \frac{z_{CG}}{\frac{1}{h_{max}} \frac{\int_0^{h_{max}} z C dz}{\int_0^{h_{max}} C dz}} \quad (11)$$

352

353

354

355

356

357

358

359

360

Eqn. 11 is a ratio of the center of gravity of the DCL to the center of gravity of the whole profile. This will give a measure of the abnormality of the DCL peak. For example, if the entire biovolume profile followed a Gaussian distribution, then the center of gravity of the DCL would equal the center of gravity of the whole profile, and $\zeta = 1$. This would also be true if biovolume concentrations were zero everywhere except the DCL. However, if there is significant biovolume in the mixed layer, then this would shift the center of gravity of the whole profile shallower, relative to the center of gravity of just the DCL, resulting in $\zeta > 1$. Similarly, ζ will be less than one if the DCL fails to capture all of the biovolume below the mixed layer.

361 It was determined that, although the values of z_{CG} were significantly different for the
 362 June and July peaky period, the ζ values of each were approximately the same, $\zeta = 1$.
 363 Further, there appears to be a sinusoidal seasonal trend in ζ that could indicate when a
 364 bloom will occur (thick black line in Fig. 11). The bloom occurs at $\zeta = 0.64$, according
 365 to the fitted sine curve; this is also the value of ζ when averaged over the three days
 366 immediately preceding the bloom (thin black vertical line demarcates when the bloom took
 367 place, thin black horizontal line shows the prior three days averaged value of ζ). To check
 368 this trend, 2018 data from Ramsey Lake—a deep, dimictic, and eutrophic lake with a history
 369 of *Microcystis* blooms—was investigated. For profiles taken when the euphotic depth was
 370 deeper than the thermocline depth, we see a similar trend, with algal blooms occurring when
 371 ζ values dip below the approximate 0.6 threshold.

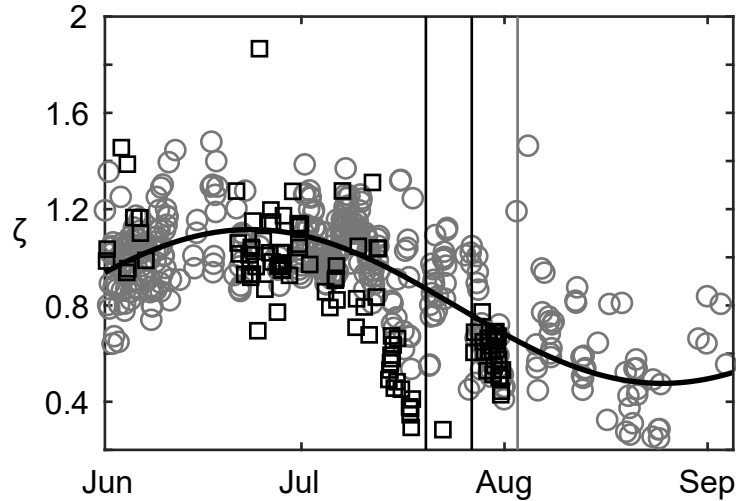


Figure 11: Seasonal trend of ζ from South Center Lake in 2017 (open gray circles) and Ramsey Lake in 2018 (open black squares). Thick black line indicates the best fit periodic function to South Lake determined to be $\zeta = 0.80 + 0.32\sin(0.05t + 7 \times 10^5)$, where t here is the Matlab serial date number ($r^2 = 0.56$, $p\text{-value} = 3.2 \times 10^{-75}$). Thin black vertical lines indicate dates of harmful algal blooms in Ramsey Lake (July 20th and 27th, 2018), and thin gray vertical line is the date of the harmful algal bloom in South Center Lake (August 3rd, 2017).

372 To further explore this, we consult individual profiles for $\zeta < 1$, $\zeta = 1$, and $\zeta > 1$ (Fig.
 373 12). When $\zeta = 1$ (Fig. 12a), as is the case for the peaky periods in June and July, we see
 374 low biovolume concentrations in the mixed layer and below the DCL. In these situations,
 375 integrating biovolume over the entire water column is essentially the same as integrating
 376 biovolume just within the DCL, hence the center of gravity of the whole profile aligns with
 377 the center of gravity of just the DCL. When $\zeta > 1$ (Fig. 12b), as is the case in between
 378 the two peaky periods in June and July, we see large concentrations of biovolume within
 379 the mixed layer relative to the biovolume concentration in the DCL. This brings the center
 380 of gravity of the whole profile shallower, when compared to the center of gravity of just
 381 the DCL. When $\zeta < 1$ (Fig. 12c), as is the case just before the surface bloom, we see a
 382 narrow DCL but a wide distance between the mixed layer depth and the thermocline depth.
 383 Using the same logic that informed our model in the previous section, a deep thermocline
 384 gives algae a larger habitable space. So even though the DCL itself occupies a narrow
 385 band immediately below the mixed layer, not insignificant populations of algae are capable
 386 of living below the DCL, thusly moving the center of gravity of the whole profile deeper
 387 compared to the center of gravity of just the DCL.

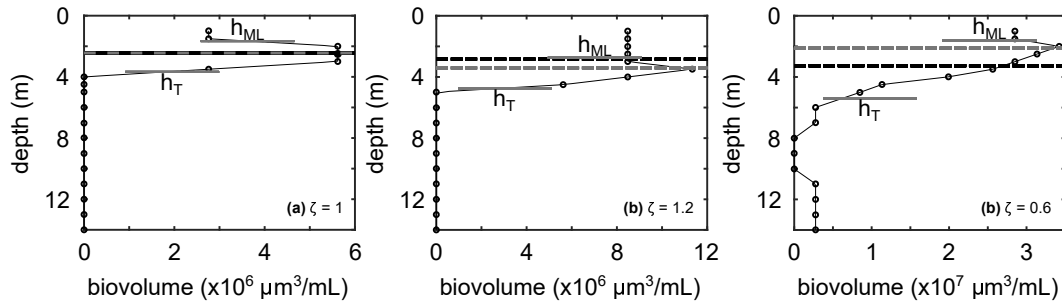


Figure 12: Examples of profiles for (a) $\zeta = 1$, profile taken July 1 2017 04:00, (b) $\zeta > 1$, profile taken June 21 2017 02:00, and (c) $\zeta < 1$, profile taken at July 31 2017 12:00. Black dashed lines indicate center of gravity of the whole biovolume profile, and gray dashed lines indicate center of gravity of the DCL.

388 Conceptually, profiles with $\zeta < 1$ appear to have a much easier journey from DCL to
 389 surface HAB compared to profiles with $\zeta \geq 1$. Recall also the phenomenon of bioconvection,
 390 in which the motion of dense algae introduces hydrodynamic instabilities into the water
 391 column (Sommer et al., 2017; Sepúlveda Steiner et al., 2019). Profiles with $\zeta \geq 1$ appear
 392 more likely to induce hydrodynamic instabilities, potentially changing the thermal structure
 393 of the lake, and inhibiting surface bloom formation.

394 The aim of this analysis is not to be conclusive, but rather provocative, in the hopes of
 395 fueling further thought and research. The center of gravity parameter is new to the field of
 396 DCL research, but its usefulness appears hopeful. If the shape of the DCL biovolume relative
 397 to the shape of the entire biovolume profile does, in fact, exhibit a predictable seasonal
 398 trend, as is suggested in Fig. 11, then this could be a missing link between predicting
 399 vertical distribution of algae and predicting harmful algal bloom formation.

400 5 Conclusions

401 A high-frequency, long-duration research station was anchored in a eutrophic and
 402 dimictic lake for the entirety of summer stratification. This research station recorded mete-
 403 orological measurements every five minutes and water quality profiles every two hours. Two
 404 key parameters were introduced to describe cyanobacterial vertical heterogeneity: C_{DCL} ,
 405 a measure of the relative peak biovolume concentration magnitude, and z_{CG} , the center of
 406 gravity of the biovolume concentration with the deep cyanobacteria layer (DCL). A stepwise
 407 regression analysis was performed to determine the dependence of these two variables on
 408 abiotic parameters of the lake.

409 A DCL was present for a large portion of the majority of the summer season. Results
 410 indicate the magnitude of the DCL peak depends on physical conditions at the thermocline,
 411 but the center of gravity of the DCL depends on physical conditions at the mixed layer.
 412 It was also shown that a large Reynolds number related to surface cooling, $Re > 5 \times 10^4$,
 413 inhibits the formation of a DCL.

414 Although definitions differed slightly, the findings presented in this paper corroborate
 415 the findings of Scofield et al. (2017) at Lake Ontario: thermal structure parameters can
 416 explain significant variability of where in the water column a DCL forms and how large
 417 the peak magnitude of the DCL gets. The machine learning algorithm developed by Xu
 418 et al. (2019) to determine key parameters and patterns of thermal and biological vertical
 419 profiles could be used to systemically determine C_{DCL} and z_{CG} from field data, in order
 420 to provide more consistent protocol and definitions between studies. This would expedite

421 research, allowing for these parameters to be modeled in a large number of lakes with
 422 different light, temperature, and nutrient regimes. The models and parameters presented in
 423 this paper not only provide phenomenological insight towards *Microcystis* lifestyles, but their
 424 utilitarian simplicity in both form and ease of measurement will also help lake water systems
 425 stakeholders with limited funds and manpower appropriately manage their resources.

426 Appendix A Vertical heterogeneity and the DCL

427 To ensure DCL definitions are physically meaningful and do not obscure biovolume
 428 vertical heterogeneities within the mixed layer, we introduce

$$429 \quad C_{ML} = \frac{C_{ML,max} - C_{ML,avg}}{C_{ML,avg}} \quad (A1)$$

430 Eqn. A1 gives the magnitude of the biovolume concentration peak within the mixed
 431 layer relative to the average concentration in the mixed layer. Our assumption is that
 432 biovolume vertical heterogeneities can only occur below the mixed layer, because mixing
 433 processes within the mixed layer will dominate any depth-specific growth or migration of
 434 cyanobacteria, thusly wiping out any possible biovolume aggregation. Values of C_{ML} close
 435 to zero will validate this assumption.

436 Results indicate an average value of $C_{ML,avg} = 0.058$, which is much lower than
 437 the average value of C_{DCL} , $C_{DCL,avg} = 0.79$ (Fig. A1). Further, there appears to be
 438 no significant difference in the distribution of C_{ML} between profiles with and without a
 439 DCL. Meaning the existence of a DCL does not impact the biovolume heterogeneity, or lack
 440 thereof, within the mixed layer. For these reasons, the authors suggest that the definition of
 441 a DCL, its bounds, and its parameters detailed in Section 2.4 accurately describe biovolume
 442 vertical heterogeneities.

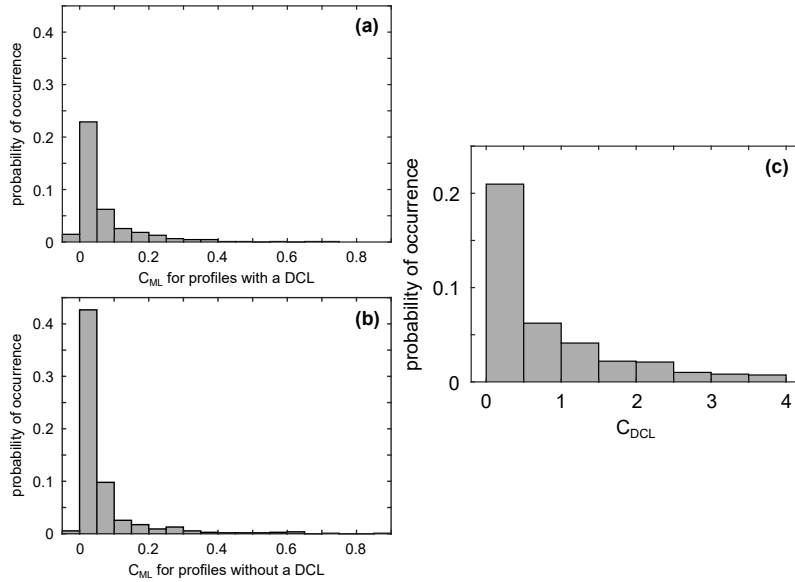


Figure A1: Histograms of (a) C_{ML} for profiles with a DCL, (b) C_{ML} for profiles without a DCL, and (c) C_{DCL} . There appears to be no discernible difference in C_{ML} distribution between profiles with and without a DCL. The largest value C_{ML} takes for all profiles is about 0.9, or a 90% increase in peak value from the mean value. This is much lower than the largest value of C_{DCL} , which is around 4.

443 **Appendix B Nutrients**

444 Nutrient grab samples were taken on an approximately weekly basis to quantify nitrate (NO_3^-) and phosphate (PO_4^{3-}) concentrations. Nitrate concentrations were below the
 445 detection limit of 0.02 mg/L for all depths for the entire summer season, and phosphate
 446 concentrations at depths of 1m, 3m, 6m, and 10m are shown in Fig. B1. Even at the
 447 lowest recorded phosphate concentration of 0.02 mg/L, the highest N:P ratio was 1, indi-
 448 cating nitrogen was likely limiting *Microcystis* growth during the entire monitoring period
 449 (Wurtsbaugh et al., 2019). However, Marinho et al. (2007) demonstrated that although
 450 N:P ratios less than 14 are correlated with *Microcystis* dominance in the field, this is likely
 451 a result of *Microcystis* dominance and not a cause (Fujimoto et al., 1997). Surface level
 452 concentrations of phosphate (1m data) remain consistently low until mid-September, well
 453 after the surface bloom of early August had formed and dissipated. The highest concentra-
 454 tions of phosphate occur in mid-July, after the July subsurface peaky period but before the
 455 August surface bloom. The phosphate profile changed from relatively uniform to almost
 456 monotonically increasing with depth in a matter of a week during this same time. However,
 457 this change in shape of the phosphate profile led to no distinguishable change in the shape
 458 of the biovolume profile. For these reasons, we suggest that nutrients played a secondary
 459 role in the vertical heterogeneity of *Microcystis* in South Center Lake for the summer 2017
 460 season. Namely, the nutrient conditions of South Center Lake allowed *Microcystis* to thrive,
 461 but did not control vertical distribution of cells.
 462

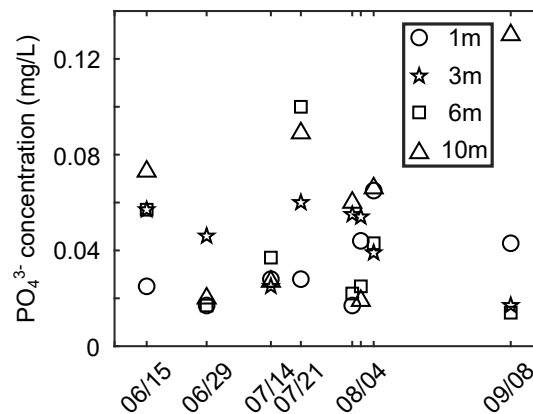


Figure B1: Phosphate concentrations (from grab samples) time series at location of research station. Circles indicate phosphate concentration at 1m, stars at 3m, squares at 6m, and triangles at 10m. Sampling dates shown on x axis.

463 **Acknowledgments**

464 Data archiving is underway at the Data Repository for University of Minnesota. Funding was
 465 provided by the Legislative-Citizen Commission on Minnesota Resources and the National
 466 Science Foundation Graduate Research Funding Program. The authors wish to thank the
 467 Minnesota Pollution Control Agency for their supplemental data provided that was used
 468 to validate research station and grab sample measurements. Finally, a special thank you
 469 goes out to Jiaqi You, for providing guidance and conducting lab analyses of grab samples;
 470 Dr. Shahram Missaghi, for help with outreach and coordination; and Dr. Anne Ahlvers-
 471 Wilkinson, for jump-starting the entire project.

References

472

473

474

475

476

477

478

479

480

481

482

483

484

485

486

487

488

489

490

491

492

493

494

495

496

497

498

499

500

501

502

503

504

505

506

507

508

509

510

511

512

513

514

515

516

517

518

519

520

521

522

523

524

525

526

- Bormans, M., Sherman, B., & Webster, I. (1999). Is buoyancy regulation in cyanobacteria an adaptation to exploit separation of light and nutrients? *Marine and Freshwater Research*, *50*(8), 897–906.
- Brooks, A. S., & Torke, B. G. (1977). Vertical and seasonal distribution of chlorophyll a in lake michigan. *Journal of the Fisheries Board of Canada*, *34*(12), 2280–2287.
- Cao, H.-S., Kong, F.-X., Luo, L.-C., Shi, X.-L., Yang, Z., Zhang, X.-F., & Tao, Y. (2006). Effects of wind and wind-induced waves on vertical phytoplankton distribution and surface blooms of microcystis aeruginosa in lake taihu. *Journal of Freshwater Ecology*, *21*(2), 231–238.
- Cullen, J. J. (1982). The deep chlorophyll maximum: comparing vertical profiles of chlorophyll a. *Canadian Journal of Fisheries and Aquatic Sciences*, *39*(5), 791–803.
- Cullen, J. J. (2015). Subsurface chlorophyll maximum layers: enduring enigma or mystery solved?
- Engel, L., Valley, R., & Vanderbosch, D. (2011). *Sentinel lake assessment report south center lake (13-0027) chisago county, minnesota* (Tech. Rep.). Minnesota Pollution Control Agency and Minnesota Department of Natural Resources.
- Fogg, G., & Walsby, A. (1971). Buoyancy regulation and the growth of planktonic blue-green algae. *Internationale Vereinigung für Theoretische und Angewandte Limnologie: Mitteilungen*, *19*(1), 182–188.
- Fujimoto, N., Sudo, R., Sugiura, N., & Inamori, Y. (1997). Nutrient-limited growth of microcystis aeruginosa and phormidium tenue and competition under various n: P supply ratios and temperatures. *Limnology and Oceanography*, *42*(2), 250–256.
- Ganf, G., & Oliver, R. (1982). Vertical separation of light and available nutrients as a factor causing replacement of green algae by blue-green algae in the plankton of a stratified lake. *The Journal of Ecology*, 829–844.
- Hozumi, A., Ostrovsky, I., Sukenik, A., & Gildor, H. (2019). Turbulence regulation of microcystis surface scum formation and dispersion during a cyanobacteria bloom event. *Inland Waters*, 1–20.
- Huisman, J., Codd, G. A., Paerl, H. W., Ibelings, B. W., Verspagen, J. M., & Visser, P. M. (2018). Cyanobacterial blooms. *Nature Reviews Microbiology*, *16*(8), 471.
- Huisman, J., Thi, N. N. P., Karl, D. M., & Sommeijer, B. (2006). Reduced mixing generates oscillations and chaos in the oceanic deep chlorophyll maximum. *Nature*, *439*(7074), 322.
- Imberger, J. (1985). The diurnal mixed layer. *Limnology and oceanography*, *30*(4), 737–770.
- Liu, M., Ma, J., Kang, L., Wei, Y., He, Q., Hu, X., & Li, H. (2019). Strong turbulence benefits toxic and colonial cyanobacteria in water: A potential way of climate change impact on the expansion of harmful algal blooms. *Science of The Total Environment*.
- Marinho, M. M., et al. (2007). Influence of n/p ratio on competitive abilities for nitrogen and phosphorus by microcystis aeruginosa and aulacoseira distans. *Aquatic Ecology*, *41*(4), 525–533.
- Marti, C. L., Imberger, J., Garibaldi, L., & Leoni, B. (2016). Using time scales to characterize phytoplankton assemblages in a deep subalpine lake during the thermal stratification period: Lake Isèo, Italy. *Water Resources Research*, *52*(3), 1762–1780.
- Medrano, E. A., Uittenbogaard, R., Pires, L. D., Van De Wiel, B., & Clercx, H. (2013). Coupling hydrodynamics and buoyancy regulation in microcystis aeruginosa for its vertical distribution in lakes. *Ecological Modelling*, *248*, 41–56.
- O’Neil, J., Davis, T., Burford, M., & Gobler, C. (2012). The rise of harmful cyanobacteria blooms: the potential roles of eutrophication and climate change. *Harmful algae*, *14*, 313–334.
- Paerl, H. W., & Huisman, J. (2008). Blooms like it hot. *Science*, *320*(5872), 57–58.
- Pollard, R. T., Rhines, P. B., & Thompson, R. O. (1972). The deepening of the wind-mixed layer. *Geophysical & Astrophysical Fluid Dynamics*, *4*(1), 381–404.
- Read, J. S., Hamilton, D. P., Jones, I. D., Muraoka, K., Winslow, L. A., Kroiss, R., . . . Gaiser, E. (2011). Derivation of lake mixing and stratification indices from high-

- 527 resolution lake buoy data. *Environmental Modelling & Software*, 26(11), 1325–1336.
- 528 Reynolds, C. S., Oliver, R. L., & Walsby, A. E. (1987). Cyanobacterial dominance: the role
529 of buoyancy regulation in dynamic lake environments. *New Zealand journal of marine
530 and freshwater research*, 21(3), 379–390.
- 531 Sanful, P. O., Otu, M. K., Kling, H., & Hecky, R. E. (2017). Occurrence and seasonal
532 dynamics of metalimnetic deep chlorophyll maximum (dcm) in a stratified meromictic
533 tropical lake and its implications for zooplankton community distribution. *Internation-
534 al Review of Hydrobiology*, 102(5-6), 135–150.
- 535 Scofield, A. E., Watkins, J. M., Weidel, B. C., Luckey, F. J., & Rudstam, L. G. (2017). The
536 deep chlorophyll layer in lake ontario: extent, mechanisms of formation, and abiotic
537 predictors. *Journal of Great Lakes Research*, 43(5), 782–794.
- 538 Sepúlveda Steiner, O., Bouffard, D., & Wüest, A. (2019). Convection-diffusion competition
539 within mixed layers of stratified natural waters. *Geophysical Research Letters*, 46(22),
540 13199–13208.
- 541 Somavilla, R., Rodriguez, C., Lavín, A., Vilorio, A., Marcos, E., & Cano, D. (2019).
542 Atmospheric control of deep chlorophyll maximum development. *Geosciences*, 9(4),
543 178.
- 544 Sommer, T., Danza, F., Berg, J., Sengupta, A., Constantinescu, G., Tokyay, T., ... others
545 (2017). Bacteria-induced mixing in natural waters. *Geophysical Research Letters*,
546 44(18), 9424–9432.
- 547 Thomas, R., & Walsby, A. (1985). Buoyancy regulation in a strain of microcystis. *Micro-
548 biology*, 131(4), 799–809.
- 549 Thomas, R., & Walsby, A. (1986). The effect of temperature on recovery of buoyancy by
550 microcystis. *Microbiology*, 132(6), 1665–1672.
- 551 Ushijima, Y., & Yoshikawa, Y. (2020). Mixed layer deepening due to wind-induced shear-
552 driven turbulence and scaling of the deepening rate in the stratified ocean. *Ocean
553 Dynamics*, 1–8.
- 554 Wallace, B. B., Bailey, M. C., & Hamilton, D. P. (2000). Simulation of vertical position
555 of buoyancy regulating microcystis aeruginosa in a shallow eutrophic lake. *Aquatic
556 Sciences*, 62(4), 320–333.
- 557 Wilkinson, A., Hondzo, M., & Guala, M. (2020). Vertical heterogeneities of cyanobacteria
558 and microcystin concentrations in lakes using a seasonal in situ monitoring station.
559 *Global Ecology and Conservation*, 21, e00838.
- 560 Woolway, R. I., Jones, I. D., Hamilton, D. P., Maberly, S. C., Muraoka, K., Read, J. S.,
561 ... Winslow, L. A. (2015). Automated calculation of surface energy fluxes with
562 high-frequency lake buoy data. *Environmental Modelling & Software*, 70, 191–198.
- 563 Wu, J. (1971). An estimation of oceanic thermal-sublayer thickness. *Journal of Physical
564 Oceanography*, 1(4), 284–286.
- 565 Wu, X., Noss, C., Liu, L., & Lorke, A. (2019). Effects of small-scale turbulence at the air-
566 water interface on microcystis surface scum formation. *Water Research*, 167, 115091.
- 567 Wurtsbaugh, W. A., Paerl, H. W., & Dodds, W. K. (2019). Nutrients, eutrophication and
568 harmful algal blooms along the freshwater to marine continuum. *Wiley Interdisci-
569 plinary Reviews: Water*, 6(5).
- 570 Xiao, M., Li, M., & Reynolds, C. S. (2018). Colony formation in the cyanobacterium
571 microcystis. *Biological Reviews*, 93(3), 1399–1420.
- 572 Xu, W., Collingsworth, P. D., & Minsker, B. (2019). Algorithmic characterization of
573 lake stratification and deep chlorophyll layers from depth profiling water quality data.
574 *Water Resources Research*.
- 575 Yao, B., Liu, Q., Gao, Y., & Cao, Z. (2017). Characterizing vertical migration of micro-
576 cystis aeruginosa and conditions for algal bloom development based on a light-driven
577 migration model. *Ecological research*, 32(6), 961–969.
- 578 Zhu, W., Feng, G., Chen, H., Wang, R., Tan, Y., & Zhao, H. (2018). Modelling the
579 vertical migration of different-sized microcystis colonies: coupling turbulent mixing
580 and buoyancy regulation. *Environmental Science and Pollution Research*, 25(30),
581 30339–30347.